ADVANCED MATERIALS
www.advmat.de

Nanoporous Walls on Macroporous Foam: Rational Design of Electrodes to Push Areal Pseudocapacitance

*Cao Guan, Xianglin Li, Zilong Wang, Xiehong Cao, Cesare Soci, Hua Zhang, and Hong Jin Fan**

The construction of high-capacitance electrochemical energy storage devices such as supercapacitors and lithium ion batteries has drawn worldwide attention as a result of the fossil-fuel crisis and the ever-increasing demands for renewable energy.[1,2] Supercapacitors, also known as electrochemical capacitors, are considered the most promising energy storage devices owing to their high power densities and long lifespan.[3–5] The fast charge and discharge capability make supercapacitors favorable for applications in hybrid vehicles, portable electronics, and backup energy systems.[6–10] Carbonaceous materials, including carbon nanotubes and graphene, are being widely studied as alternatives to conventional graphites.[2,11–14] However, carbon-based materials usually show low energy density as they store charges electrostatically at their surfaces, so they have intrinsically low specific areal capacitance (C_a) in the range of 10–40 μF cm^{-2}. Transition metal oxides/hydroxides store charges with surface faradaic (redox) reactions, which enable higher energy density compared to carbon. Metal oxides/hydroxides such as MnO_2, NiO, $Ni(OH)_2$, CoO_x and their compounds have recently come into focus in the design of high-energy-density charge-storage materials.[15–27] Despite these efforts, practical energy storage applications still require higher specific capacitance. One way out is to design nanometer-scale electrode materials with very large surface areas and structural stability. In this context, porous nanostructures are of great interest because they can reduce ionic and electronic diffusion distance and provide large electrode/electrolyte contact area. For example, porous Ni and Au electrodes as current collectors have recently been reported, which significantly improve the specific capacitance when covered with the pseudoactive material MnO_2.[28,29] Also, nanoporous graphene electrodes with ~4 nm pores drastically enhance the specific capacitance up to 166 F g^{-1}.[30] For metal oxides, a highly porous nanostructure should also boost the areal capacitance. In most of the previous reports on pseudocapacitive metal oxide nanostructures, the electrode surfaces appear "porous" but only on a relatively large size scale (>100 nm). A truly high-order porous pseudocapacitive metal oxide nanostructure has scantly been reported.

Based on the above considerations, we intend to develop highly nanoporous metal oxides as a high areal-capacitance supercapacitor electrode. Specifically, porous CoO nanowalls have been fabricated using a revised hydrothermal method on commercial macroporous nickel foam substrate. The CoO nanowalls are quasi aligned on the nickel surface, which is believed to allow easy access of electrolyte to the entire walls. An areal capacitance of ~2.3 F cm^{-2} is achieved with this nanoporous walls@macropous foam electrode. Furthermore, the nanowall surfaces can be made more rough and active by further deposition of new pseudocapacitive nanomaterials. As exemplified by $Ni(OH)_2$ nanolayers, the combination leads to a giant enhancement of areal capacitance up to ~11.5 F cm^{-2}. Here we stress the synergy effect of the hybrid metal oxides. With a rational combination of two types of materials and/or nanostructures, enhanced electrochemical performance compared to their single-component constituents are expected and have recently been demonstrated in some oxide-based systems.[31–33] It is believed that the nanoporous metal oxides on metal foams demonstrated in the present work, or more generally on carbon wovens,[34] will be a promising type of electrodes for supercapacitors.

The crystal phase of the sample was characterized using standard X-ray diffraction (XRD). The XRD pattern in Figure S1a in the Supporting Information of the as-prepared sample matches well the reported pattern of $Co(OH)_2$ (JCPDS card no: 74-1057).[35] The thermal annealing turned the $Co(OH)_2$ into CoO phase, as can be seen from the lower branch in Figure S1a (JCPDS card no: 48-1719).[36] This transformation is further verified by Fourier transform infrared (FTIR) spectra in Figure S1b. Before annealing, two peaks observed in the range 500–700 cm^{-1} represent v-Co–O;[37] peaks at 1199 and 1384 cm^{-1} are associated with NO_3^-;[38] two peaks at 1039 and 1486 cm^{-1} are correlated with CO_3^{2-}; peaks at 2870 and 2934 cm^{-1} are assigned to C–H vibrations; and the other two peaks at 1620 and 3644 cm^{-1} are associated with the vibrations of H_2O.[38,39] After annealing, most of these peaks disappeared while the Co–O peaks still remained strong. This further verifies the transformation of $Co(OH)_2$ to CoO.

The scanning electron microscopy (SEM) images in **Figures 1**a–c show the aligned CoO nanowalls directly on the nickel foam. The macroporous nickel foam is covered with

C. Guan, X. L. Li, Z. L. Wang, Prof. C. Soci, Prof. H. J. Fan
Division of Physics and Applied Physics
School of Physical and Mathematical Sciences
Nanyang Technological University
Singapore 637371, Singapore
E-mail: fanhj@ntu.edu.sg
C. Guan, Prof. H. J. Fan
Energy Research Institute @ NTU (ERIAN)
Nanyang Technological University
50 Nanyang Drive, Singapore 637553, Singapore
X. H. Cao, Prof. H. Zhang
School of Materials Science and Engineering
Nanyang Technological University
Singapore 639798, Singapore

DOI: 10.1002/adma.201104295

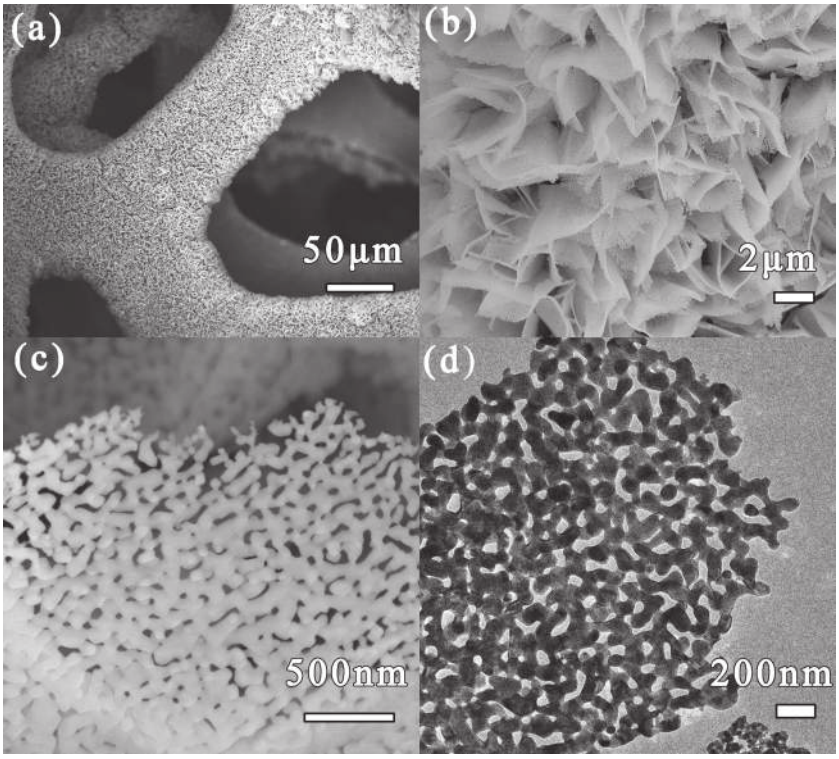

Figure 1. a–c) SEM images of the CoO nanowalls grown directly on the nickel foam. d) TEM image of an individual piece of CoO nanowall.

the CoO nanostructures. Photographs and a large-scale SEM image of the sample can be seen in the Supporting Information (Figures S2 and S3). Figure 1b indicates that the nanowalls with a size of 4–5 μm are aligned vertically on the nickel foam and have a cross-linked character. The overall alignment is beneficial to the charge transport and ion diffusion without the necessity of binder blocks. The magnified image of an individual nanowall in Figure 1c reveals the highly porous structure with pore diameters around or below 100 nm. The transmission electron microscopy (TEM) image in Figure 1d provides further information on the porous structure, which is that a typical nanowall is composed of many small nanobricks tightly interconnected with each other. Therefore, the annealing step converted $Co(OH)_2$ to highly porous CoO,[39, 40] during which the architecture of the nanowalls was well preserved.

To evaluate the supercapacitor applications of these porous nanostructures, the electrochemical properties were investigated. The redox reaction of CoO in the electrolyte as revealed by the cyclic voltammetry (CV) curve is shown in Figure S4a (Supporting Information). **Figure 2**a shows the charge–discharge behavior of the CoO nanowalls between 0 and 0.55 V at different current densities. The specific capacitance is calculated as

$$C = It/(m\Delta V) \quad (1)$$

and areal capacitance is calculated as

$$C_a = It/(S\Delta V) \quad (2)$$

where I is the discharge current, t the discharge time, m the mass of the active material, ΔV the voltage drop upon discharging, and S the geometrical area of the electrode. From Equation (1), the CoO nanowalls displayed specific capacitances of 364.2, 461.7, 515.6, and 539.8 F g^{-1} at discharge currents of 9.30, 4.65, 2.33, and 1.17 A g^{-1}, respectively, which are much higher than that (307 F g^{-1} at 4.55 A g^{-1}) of CoO nanowires reported previously.[32] This increase is attributed to the porous structure of the walls, which provides more surface area in contact with the electrolyte, so more active material can effectively contribute to the capacitance. Based on Equation (2), the areal capacitance of the CoO nanowalls is 2.32 F cm^{-2}. It is worth noting that nickel foam itself could influence the final CV curve with a small capacitance contribution.[32] In order to illustrate the contribution of the active material, in all of the following results the small contribution from the Ni foam was subtracted.

The charge–discharge cyclic stability of the CoO nanowalls was tested further. As shown in Figure 2b, after 5000 charge–discharge cycles at a current density of 4.65 A g^{-1}, the structure shows only a small loss of capacitance (less than 5%). The good long-term electrochemical stability is also demonstrated by comparing the XRD patterns of the CoO nanowalls before and after 5000 cycles (inset in Figure 2b): after long-time cycling little change of the CoO peaks was observed and no other impurity was apparent. The morphology of the CoO nanowalls was checked after 5000 cycles (see SEM image in Figure S4b, Supporting Information), which showed that the porous structure was fully maintained and no obvious changes were observed. Therefore, owing to its highly porous and crystalline structure and the direct connection with the macroporous nickel foam, the CoO nanowalls exhibited not only high capacitance but also long cycling stability; both are key parameters for commercial applications in high-demand energy storage.

To further push the areal capacitance, we now consider the hybridization with an additional metal oxide. The aligned and cross-linked CoO nanowalls can serve as a robust and conductive scaffold for the loading of additional pseudoactive nanomaterial. To achieve synergy, the newly introduced material would be required to fulfill the following requirements: to contribute effective specific capacitance, to enlarge the surface area but not to prevent contact between the CoO nanowalls and ions in the electrolyte, and to maintain the structural integrity. With these aims, electrodeposition was chosen as a convenient and controllable method to coat the surface of CoO with another pseudocapacitive metal oxide. In our study, we obtained a few hybrid nanostructures by changing the solution for electrodeposition, for example, MnO_2 and $Ni(OH)_2$. Both of these materials show a flake structure and thus are promising as a supercapacitor electrode material. It is expected that these *porous + flake* hybrid nanoscale metal oxides will also be useful in lithium ion batteries and gas sensing. In the following we take $Ni(OH)_2$ as an example for discussion.

Adv. Mater. **2012**,
DOI: 10.1002/adma.201104295

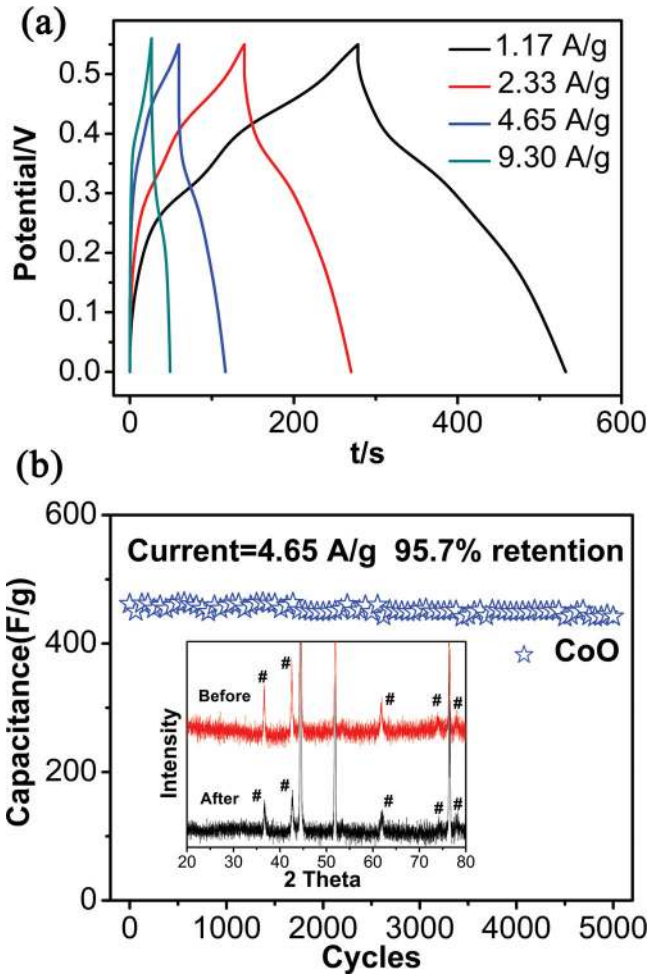

Figure 2. a) Charge–discharge curves of the CoO nanowalls at different current densities. b) Cycling performance of the CoO nanowalls. Inset: XRD patterns before cycling and after 5000 cycles, showing the structural preservation.

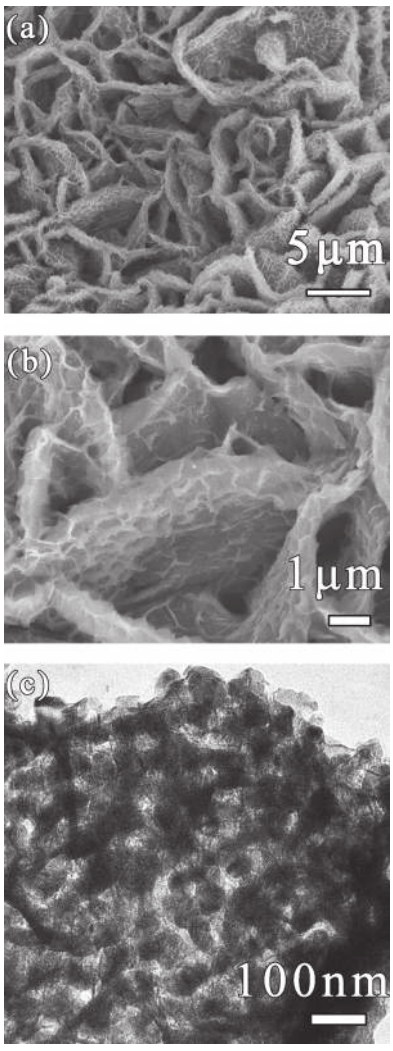

Figure 3. SEM (a,b) and TEM (c) images of the hybrid structure of CoO@$Ni(OH)_2$ obtained after 15 min electrodeposition.

XRD was performed on the sample after $Ni(OH)_2$ electrodeposition on the CoO nanowalls (Figure S5, Supporting Information). New peaks appearing in the XRD pattern of the hybrid structure can be well indexed to α-$Ni(OH)_2$.[41,42] **Figure 3** shows the morphology of the nanowalls after 15 min electrochemical deposition. The SEM images show that leaf-like $Ni(OH)_2$ thin layers cover uniformly the surface of the CoO nanowalls. It is possible that the pores of the CoO nanowall are also filled with the thin layers, as seen from the TEM image.

The evolution of the nanolayers was examined by conducting time-dependent growth experiments. SEM and TEM images of the sample after different electrodeposition times are shown in the Supporting Information (Figures S6 and S7). One can clearly see that the size and coverage of the $Ni(OH)_2$ nanolayers depends on the deposition time; they grow individually and then percolate until full coverage of the CoO nanowall surface is achieved. Correspondingly, the variation of the capacitance with electrodeposition time is examined and plotted in Figure S8 (Supporting Information). The highest capacitance corresponds to 15 min deposition of $Ni(OH)_2$. These data clearly illustrate the convenience of electrodeposition in tailoring the nanoelectrode surface.

The CoO@$Ni(OH)_2$ hybrid nanostructure demonstrates enhanced electrochemical properties as a supercapacitor electrode. For a direct comparison, the CV curves under the same scan rate and the areal capacitances of pure CoO, $Ni(OH)_2$ and hybrid CoO@$Ni(OH)_2$ are depicted in **Figure 4**. In Figure 4a, the red curve shows the CV behavior of the hybrid electrode with 15 min electrodeposition at a scan rate of 2 mV s^{-1}. In comparison with the CV curves of the CoO nanowalls (blue line) and $Ni(OH)_2$ nanolayers directly deposited on the nickel foam (black curve), the enclosed area is greatly increased, indicative of larger capacitance. From Figure 4b, one can see that the capacitance of the hybrid electrode is even ~3 times the simple addition of the two components. For example, the areal capacitance reaches 11.49 F cm^{-2} at a current density of 5 mA cm^{-2}, whereas the values for the individual CoO and $Ni(OH)_2$ are 2.3 and 1 F cm^{-2}. This value of areal capacitance (11.49 F cm^{-2}) of

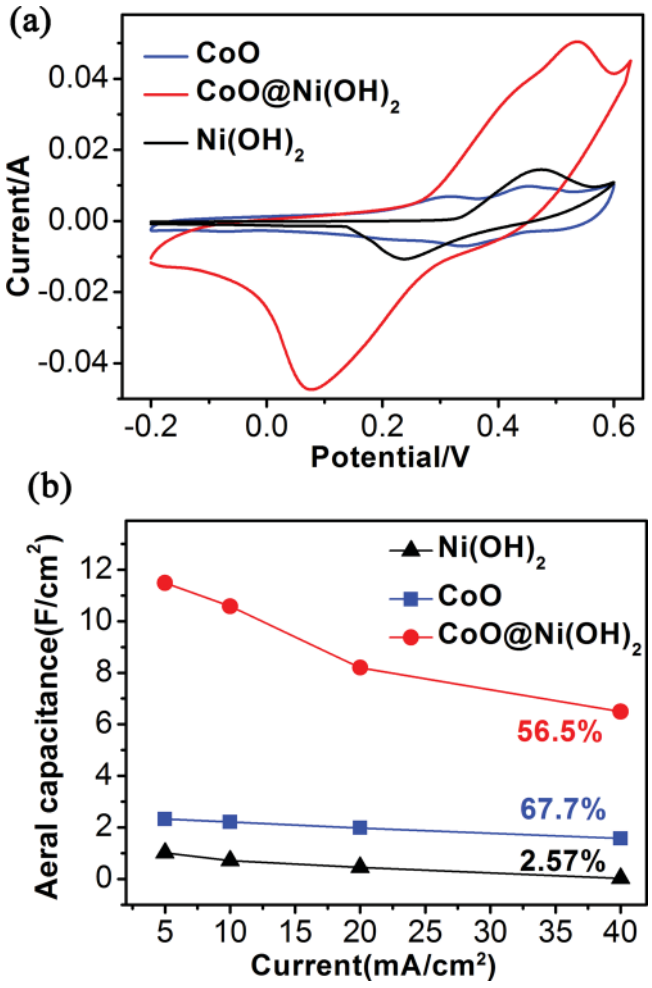

Figure 4. a) Comparison of the charge–discharge behavior between CoO nanowall electrode and CoO@$Ni(OH)_2$ hybrid electrode at the same current density. The scan rate is 2 mV s^{-1}. b) Comparison of the areal capacitance of the three structures $Ni(OH)_2$, CoO, and CoO@$Ni(OH)_2$ at various current densities. The percentages show the capacitance retention when the current was increased from 5 to 40 mA cm^{-2}.

the CoO@$Ni(OH)_2$ hybrid structure is, to the best of our knowledge, the highest value reported for metal oxides/hydroxides with a high mass loading.[19,31,35,43,44]

The capacitance improvement can also be seen from the charge–discharge curves (see Figure S9a, Supporting Information). At the same current density of 10 mA cm^{-2}, the capacitance of the hybrid structure is increased ~4.8 times compared to pure CoO nanowalls (with only a small amount of $Ni(OH)_2$ deposited, corresponding to a 12.6% mass increase). The hybrid structure has specific capacitances of 1340.9, 1694.2, 2185.9, and 2374.0 F g^{-1} at discharge currents of 8.26, 4.13, 2.07, and 1.03 A g^{-1}, respectively (see Figure S9b). The highest specific capacitance reported so far is 3152 F g^{-1} by G. W. Yang et al.,[43] but the corresponding C_a is only ~1.58 F cm^{-2}.

The large improvement in areal capacitance in our study could be attributed to a synergy between the two oxides. The core CoO nanowalls with excellent electrochemical stability and high surface area act as a robust and conductive host for $Ni(OH)_2$; the addition of $Ni(OH)_2$ nanolayers not only contributes another effective redox reaction to the capacitance (reaction between Ni^{2+}/Ni^{3+} and OH^- anions),[42–44] but also enlarges the surface area of the whole electrode. The surface areas of the hybrid electrode (15 min electrodeposition) measured by the Brunauer–Emmett–Teller (BET) method is 9.12 m^2 g^{-1}, as compared to 7.66 m^2 g^{-1} for the CoO nanowall-covered nickel foam and 0.01 m^2 g^{-1} for the bare nickel foam.

The capacitances generally drop sharply with increasing discharge rate. In our case, Figure 4b shows that the electrode of $Ni(OH)_2$ nanolayers directly deposited on nickel foam had only 2.57% retention when the discharge current increased by a factor of eight from 5 to 40 mA cm^{-2}. In contrast, for the hybrid structure, 56.5% of the capacitance (6.49 F cm^{-2}) is maintained, which supports the idea that a positive role is played by the porous CoO nanowalls in the overall supercapacitor performance.

The synergy can also be seen from the cycling performance. As previously reported[42,43] and also shown by our own study, the $Ni(OH)_2$ nanolayers directly deposited on nickel foam are not electrochemically stable and have poor cycling behavior. When they are hybridized with the CoO nanowalls, it is found that the capacitance of the coupled electrode decays much more slowly than that of the pure $Ni(OH)_2$ (see data in Figure S10, Supporting Information). When compared at a current density of 30 mA cm^{-2}, the hybrid electrode has 68.9% capacitance retention after 5000 cycles, whereas the $Ni(OH)_2$-nanolayer electrode has only 52.0% after 500 cycles. This implies that highly pseudocapacitive $Ni(OH)_2$ can be more stable when coupled with another oxide rather than directly deposited on metallic current collectors.

In summary, highly porous CoO nanowalls were fabricated directly on 3D macroporous nickel foam for application as a pseudocapacitor electrode. A relatively high areal capacitance of ~2.3 F cm^{-2} was achieved because of the porous structure. By grafting the porous nanowalls with another pseudocapacitive oxide, the areal capacitance can be further boosted, up to ~11.5 F cm^{-2} in the case of electrochemically deposited $Ni(OH)_2$ nanolayers. Such an ultrahigh areal capacitance of the nanohybrid electrode is ascribed to the much increased surface area caused by its hierarchically porous structure, as well as a possible synergetic effect between the two oxides. Similarly, we have also achieved electrodeposition of MnO_2 nanoflakes on the porous CoO nanowalls (data not shown here). This type of hybrid 3D nanostructure with cost-effective fabrication and promising electrochemical performance shows great potential for electrochemical energy storage applications.

Experimental Section

Synthesis: The 3D hybrid electrode material was prepared by a simple two-step process, which can be easily scaled up. First, the CoO nanowalls were synthesized on nickel foam by a hydrothermal process as reported. In detail, nickel foam (20 mm × 50 mm × 0.1 mm, 100 ppi (pores per inch), 330 g m^{-2}, Changsha Lyrun Material Co., Ltd., P. R. of China) was pretreated with concentrated HCl solution, absolute ethanol, and deionized water, each for 5 min, to ensure its surface was well cleaned. Then the nickel foam with a part left as supporting electrode for electrodeposition/testing was put in a Teflon

Adv. Mater. **2012**,
DOI: 10.1002/adma.201104295

(polytetrafluoroethylene)-lined stainless steel autoclave with a 50 mL homogeneous solution containing 5 mmol $Co(NO_3)_2{\cdot}6H_2O$ and 10 mmol HMT (hexamethylene tetramine). After 8 h growth at 95 °C, the as-prepared precursors were annealed under a constant flow of argon (50 sccm) at 450 °C for 2 h. Second, the nickel foam with CoO nanowalls (mass loading: 4.3 mg cm^{-2}) was used as a working electrode for electrodeposition of $Ni(OH)_2$, which was carried out using a Chenhua model CHI 760D Electrochemical Workstation (Shanghai), with a three-electrode setup consisting of Ag/AgCl and a platinum plate as reference and counter electrode, and with an aqueous solution of 0.1 M $Ni(NO_3)_2$ as the electrolyte. The electrodeposition experiments were carried out at a constant current of 1 mA with different time ranges from 2 to 30 min to ensure the conformal coating of $Ni(OH)_2$ nanostructures on CoO nanowalls, and the mass of deposited $Ni(OH)_2$ could be calculated by Faraday's law. After deposition, the as-prepared CoO@$Ni(OH)_2$ electrode was washed with water several times and then placed in a vacuum oven at 60 °C for 2 h. The mass of deposited $Ni(OH)_2$ nanomaterial was again obtained by the weight difference before and after electrodeposition.

Material characterization: Samples were characterized by powder XRD (Bruker D-8 Avance), SEM (JSM-6700F, 10.0 kV), TEM (JEM-2010FEF, 200 kV), and FTIR spectroscopy (Bruker Vertex 80V HYPERION 2000 Microscope with mercury cadmium telluride (MCT) detector). The mass of electrode materials was measured on an AX/MX/UMX Balance (Mettler Toledo, maximum = 5.1 g; $\delta = 0.001$ mg). Nitrogen adsorption/desorption isotherms were measured on a Micromeritics TriStar 3000 porosimeter (mesoporous characterization) and a Micromeritics ASAP 2020 (microporous characterization) at 77 K. All samples were outgassed at 100 °C for 6 h under vacuum before measurements were recorded. The specific surface areas were calculated using the BET method.

Electrochemical characterization: Electrochemical measurements (CHI 760D Electrochemical Workstation) were performed in a three-electrode electrochemical cell at room temperature using 1 M NaOH as the electrolyte. The nickel-foam-supported hybrid nanostructure (~1 cm^2 area) acted directly as the working electrode. A Pt plate and Ag/AgCl were used as the counter electrode and the reference electrode, respectively. All potentials were referred to the reference electrode. The weight-specific capacitance [F g^{-1}] and current rate [A g^{-1}] were calculated based on the whole mass of the two active materials, CoO and $Ni(OH)_2$.

Supporting Information

Supporting Information is available from the Wiley Online Library or from the authors.

Received: November 9, 2011
Revised: March 7, 2012
Published online:

[1] J. R. Miller, P. Simon, *Science* **2008**, *321*, 651.
[2] P. Simon, Y. Gogotsi, *Nat. Mater.* **2008**, *7*, 845.
[3] C. Liu, F. Li, L.-P. Ma, H.-M. Cheng, *Adv. Mater.* **2010**, *22*, E28.
[4] G. W. Ho, A. S. W. Wong, *Appl. Phys. A* **2007**, *86*, 457.
[5] J. Jiang, Y. Y. Li, J. P. Liu, X. T. Huang, *Nanoscale* **2011**, *3*, 45.
[6] F. Y. Cheng, J. Liang, Z. L. Tao, J. Chen, *Adv. Mater.* **2011**, *23*, 1695.
[7] J.-H. Kim, K. Zhu, Y. F. Yan, C. L. Perkins, A. Frank, *Nano Lett.* **2010**, *10*, 4099.
[8] J. Liu, G. Z. Cao, Z. G. Yang, D. H. Wang, D. Dubois, X. D. Zhou, G. L. Graff, L. R. Pederson, J. G. Zhang, *ChemSusChem* **2008**, *1*, 676.
[9] L. Li, T. Y. Zhai, H. B. Zeng, X. S. Fang, Y. Bando, D. Golberg, *J. Mater. Chem.* **2011**, *21*, 40.
[10] X. Zhao, B. M. Sanchez, P. J. Dobson, P. S. Grant, *Nanoscale* **2011**, *3*, 839.
[11] S. J. Guo, S. J. Dong, *Chem. Soc. Rev.* **2011**, *40*, 2644.
[12] E. Raymundo-Pinero, M. Cadek, F. Beguin, *Adv. Funct. Mater.* **2009**, *19*, 1032.
[13] C. J. Yu, C. Masarapu, J. P. Rong, B. Q. Wei, H. Q. Jiang, *Adv. Mater.* **2009**, *21*, 4793.
[14] M. Kaempgen, C. K. Chan, J. Ma, Y. Cui, G. Gruner, *Nano Lett.* **2009**, *9*, 1872.
[15] X. H. Xia, J. P. Tu, Y. Y. Mai, X. L. Wang, C. D. Gu, X. B. Zhao, *J. Mater. Chem.* **2011**, *21*, 9319.
[16] J. Jiang, J. P. Liu, R. M. Ding, J. H. Zhu, Y. Y. Li, A. Z. Hu, X. Li, X. T. Huang, *ACS Appl. Mater. Interfaces* **2011**, *3*, 99.
[17] Y. Y. Liu, M. Clark, Q. F. Zhang, D. M. Yu, D. W. Liu, J. Liu, G. Z. Cao, *Adv. Energy Mater.* **2011**, *1*, 194.
[18] R. Liu, S. B. Lee, *J. Am. Chem. Soc.* **2008**, *130*, 2942.
[19] H. L. Wang, H. S. Casalongue, Y. Y. Liang, H. J. Dai, *J. Am. Chem. Soc.* **2010**, *132*, 7472.
[20] Y. G. Guo, J. S. Hu, L. J. Wan, *Adv. Mater.* **2008**, *20*, 2878.
[21] M. G. Kim, J. Cho, *Adv. Funct. Mater.* **2009**, *19*, 1497.
[22] T. Y. Wei, C. H. Chen, H. C. Chien, S. Y. Lu, C. C. Hu, *Adv. Mater.* **2010**, *22*, 347.
[23] Y. G. Li, P. Hasin, Y. Y. Wu, *Adv. Mater.* **2010**, *22*, 1926.
[24] Z. S. Wu, D. W. Wang, W. C. Ren, J. P. Zhao, G. M. Zhou, F. Li, H. M. Cheng, *Adv. Funct. Mater.* **2010**, *20*, 3595.
[25] L.-Q. Mai, F. Yang, Y.-L. Zhao, X. Xu, L. Xu, Y. Z. Luo, *Nat. Commun.* **2011**, *2*, 381.
[26] Y. Gao, S. Chen, D. Cao, G. Wang, J. Yin, *J. Power Sources* **2010**, *195*, 1757.
[27] X. Qing, S. Liu, K. Huang, K. Lv, Y. Yang, Z. Lu, D. Fang, X. Liang, *Electrochim. Acta* **2011**, *56*, 4985.
[28] H. G. Zhang, X. D. Yu, P. V. Braun, *Nat. Nanotechnol.* **2011**, *6*, 277.
[29] X. Y. Lang, A. Hirata, T. Fujita, M. W. Chen, *Nat. Nanotechnol.* **2011**, *6*, 232.
[30] Y. W. Zhu, S. Murali, M. D. Stoller, K. J. Ganesh, W. W. Cai, P. J. Ferreira, A. Pirkle, R. M. Wallace, K. A. Cychosz, M. Thommes, D. Su, E. A. Stach, R. S. Ruoff, *Science* **2011**, *332*, 1537.
[31] J. P. Liu, J. Jiang, C. W. Cheng, H. X. Li, J. X. Zhang, H. Gong, H. J. Fan, *Adv. Mater.* **2011**, *23*, 2076.
[32] C. Guan, J. P. Liu, C. W. Cheng, H. X. Li, X. L. Li, W. W. Zhou, H. Zhang, H. J. Fan, *Energy Environ. Sci.* **2011**, *4*, 4496.
[33] Y. B. He, G. R. Li, Z. L. Wang, C. Y. Su, Y. X. Tong, *Energy Environ. Sci.* **2011**, *4*, 1288.
[34] Z. P. Chen, W. C. Ren, L. B. Gao, B. L. Liu, S. F. Pei, H. M. Cheng, *Nat. Mater.* **2011**, *10*, 424.
[35] V. Gupta, T. Kusahara, H. Toyama, S. Gupta, N. Miura, *Electrochem. Commun.* **2007**, *9*, 2315.
[36] J. Jiang, J. P. Liu, R. M. Ding, X. X. Ji, Y. Y. Hu, X. Li, A. Z. Hu, F. Wu, Z. H. Zhu, X. T. Huang, *J. Phys. Chem. C* **2010**, *114*, 929.
[37] N. A. M. Barakat, M. S. Khil, F. A. Sheikh, H. Y. Kim, *J. Phys. Chem. C* **2008**, *112*, 12225.
[38] Z. P. Xu, H. C. Zeng, *Chem. Mater.* **1999**, *11*, 67.
[39] J. X. Zhu, Z. Gui, *Mater. Chem. Phys.* **2009**, *118*, 243.
[40] H. Y. Liang, J. M. Raitano, L. H. Zhang, S. W. Chan, *Chem. Commun.* **2009**, 7569.
[41] G. T. Duan, W. P. Cai, Y. Y. Luo, F. Q. Sun, *Adv. Funct. Mater.* **2007**, *17*, 644.
[42] Y. F. Yuan, X. H. Xia, J. B. Wu, J. L. Yang, Y. B. Chen, S. Y. Guo, *Electrochim. Acta* **2011**, *56*, 2627.
[43] G. W. Yang, C. L. Xu, H. L. Li, *Chem. Commun.* **2008**, 6537.
[44] Z. Y. Lu, Z. Chang, W. Zhu, X. M. Sun, *Chem. Commun.* **2011**, *47*, 9651.